Dynamic Flow Modelling for Model-Predictive Wind Farm Control

Van Den Broek, Maarten J.; Wingerden, Jan Willem Van

DOI
10.1088/1742-6596/1618/2/022023

Publication date
2020

Document Version
Final published version

Published in
Journal of Physics: Conference Series

Dynamic Flow Modelling for Model-Predictive Wind Farm Control

Journal of Physics: Conference Series **1618** (2020) 022023 doi:10.1088/1742-6596/1618/2/022023

Dynamic Flow Modelling for Model-Predictive Wind Farm Control

Maarten J. van den Broek, Jan-Willem van Wingerden

Delft Center for Systems and Control, Delft University of Technology, Mekelweg 2, 2628 CD Delft, NL

E-mail: m.j.vandenbroek@tudelft.nl

Abstract. We aim to improve wind farm control for power output by building on the results from WFSim for the development of a dynamic wind farm model. This model will be part of a closed-loop, economic model-predictive control approach for wind farms. It is constructed from first principles using open-source tools to be suitable for adjoint-based optimisation of turbine yaw angles.

In a steady-state inflow configuration with two turbines, the new control model matches power expectations from high fidelity simulations in SOWFA to within 15 %. Under time-varying wind directions, it shows time delays in wake direction as inflow changes propagate through the farm with the wind speed, although the dynamics still differ from the SOWFA reference. The model runs flow simulations for a wind farm with a 3×3 array of turbines at a real-time order of magnitude on a regular laptop computer.

The new control model shows dynamic flow behaviour as wake changes propagate through the wind farm. Some further adjustments are necessary to accurately model three-dimensional flow in two dimensions. With more validation of the wake dynamics, it will be suitable for application in a new closed-loop wind farm controller.

1. Introduction

Large, densely spaced wind farms suffer from aerodynamic interaction between wind turbines. A turbine operating in the wake of another turbine has a reduced power output and increased structural loading. Control strategies considering the wind farm as a whole may incorporate wake effects that are currently not accounted for in commercially operated wind farms.

Wind turbines may be operated under yaw misalignment to redirect the downstream wake. This reduces power output for the misaligned turbine but model studies [1, 2] and wind-tunnel experiments [3] have shown improved power production for the park as a whole, as well as a reduced structural loading on downstream turbines. Field experiments confirm these findings for specific wind directions [4], although without a significant gain in annual energy production [5].

These results rely mostly on steady-state models that neglect the temporal dynamics of the flow, which means that realistic, time-varying atmospheric conditions can not be accounted for. These conditions can be included in dynamic models. Model-predictive control using adjoint-based optimisation with large-eddy simulations provides promising results, but is not suitable for real-time application [6]. As opposed to using high-fidelity simulations, control-oriented models such as WFSim [7] provide less computationally expensive flow solutions for wind farm control. Feedback control using this model has also been demonstrated to be effective for active power

control with waked wind farms [8]. Experts on wind farm control agree that development of numerical models and real-time control should be a research priority [9].

WFSim establishes a baseline for medium-fidelity wind farm modelling, but lacks flexibility for the development of new closed-loop wind farm control methods. Therefore, we build on its results to construct a dynamic control-oriented wind farm model that is more flexibly applicable, as well as suitable for adjoint-based optimisation.

We seek to consider the wind farm as a complete system and construct closed-loop control methods to generate optimal yaw set-points for individual turbines. For the development of this control approach, this paper contributes:

(i) construction of a dynamic wind farm model for control,
(ii) validation with high-fidelity simulation,
(iii) and comparison with steady-state results.

Section 2 describes the model construction, followed by the methods for verification and validation in Section 3. The results are presented in Section 4 and discussed in Section 5. Finally, Section 6 draws the main conclusions.

2. Model Development

This section positions the model within a closed-loop control strategy in Section 2.1 and describes the approach to flow modelling in Section 2.2.

2.1. Closed-Loop Control

The model is built to be a part of a closed-loop controller as illustrated in Figure 1. A series of optimal yaw controls is to be generated using an economic model-predictive control approach. State estimation allows dealing with time-varying inflow conditions and improves model correspondence with reality.

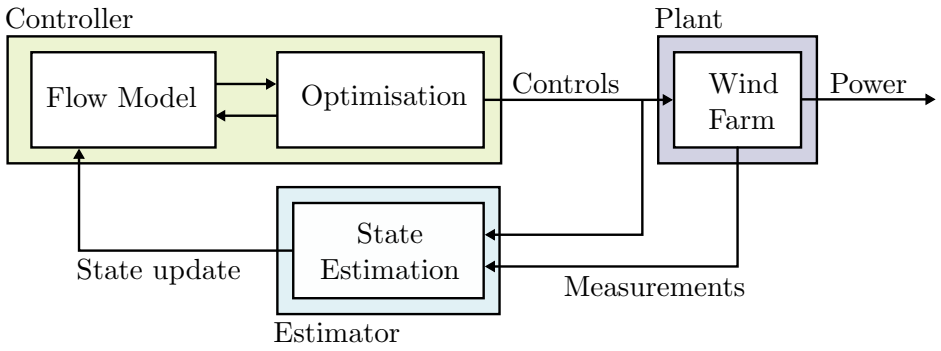

Figure 1: Closed-loop model-based wind farm control loop. This paper focuses on development of a model suitable for on-line generation of optimal control signals.

Following the line of work presented by King et al. [10] on lay-out optimisation for wind farms with steady flow solutions, the wind farm model is developed in Python using the FEniCS toolbox [11]. The separation of high-level problem definitions from computational methods facilitates fast development and flexibility in the problem definitions. Dolfin-adjoint [12] makes use of these high-level definitions to perform automated adjoint calculations that will enable efficient control optimisation.

2.2. Flow Modelling

2.2.1. Navier-Stokes We take the standard formulation of the incompressible Navier-Stokes equations for viscous flow

$$\dot{\boldsymbol{u}} + (\boldsymbol{u} \cdot \nabla)\, \boldsymbol{u} - \nu \nabla^2 \boldsymbol{u} + \frac{1}{\rho} \nabla p = \boldsymbol{f}\,, \tag{1}$$

$$\nabla \cdot \boldsymbol{u} = 0\,, \tag{2}$$

where $\boldsymbol{u}$ is the velocity vector field, p is the pressure field, $\boldsymbol{f}$ is the forcing applied to the flow, ρ is fluid density, and ν is the kinematic viscosity.

2.2.2. Temporal Discretisation The Navier-Stokes equations are discretised in time according to [13] using a discretisation that is unconditionally numerically stable, where $\boldsymbol{u}_n$ the value at time-step t_n:

$$\frac{1}{\Delta t} (\boldsymbol{u}_{n+1} - \boldsymbol{u}_n) + \mathbf{B}(\tilde{\boldsymbol{u}})\bar{\boldsymbol{u}} - \nu \nabla^2 \bar{\boldsymbol{u}} + \frac{1}{\rho} \nabla p = \boldsymbol{f}_{n+\alpha}\,, \tag{3}$$

$$\nabla \cdot \boldsymbol{u}_{n+\alpha} = 0\,, \tag{4}$$

where the intermediate velocity field $\bar{\boldsymbol{u}}$ is given by

$$\bar{\boldsymbol{u}} = \boldsymbol{u}_{n+\alpha} := \alpha \boldsymbol{u}_{n+1} + (1-\alpha)\, \boldsymbol{u}_n\,, \qquad \text{for } \alpha \in [0,1]\,. \tag{5}$$

The convective term $\boldsymbol{B}$ is formulated in a skew-symmetric form

$$\begin{gathered} \boldsymbol{B}(\tilde{\boldsymbol{u}})\bar{\boldsymbol{u}} := \frac{1}{2}[(\tilde{\boldsymbol{u}} \cdot \nabla)\bar{\boldsymbol{u}} + \nabla(\bar{\boldsymbol{u}} \otimes \tilde{\boldsymbol{u}})]\,, \\ \text{where } \tilde{\boldsymbol{u}} = \boldsymbol{u}_{n+\theta}\,, \qquad \text{for } \theta \leq 0\,. \end{gathered} \tag{6}$$

This discretisation is linear in the time-step for $\alpha = \frac{1}{2}$ and $\theta = -\frac{1}{2}$.

2.2.3. Spatial discretisation The finite-element method is used for spatial discretisation with the Taylor-Hood element. This exists in the mixed function space $W = V \times P$, where V is a second order function space and P is first order. Multiplication of the Navier-Stokes discretisation by test functions $v \in V$ and $q \in P$, followed by integration by parts over the domain, yields the variational form of the problem:

$$\langle \boldsymbol{u}_{n+1} - \boldsymbol{u}_n, \boldsymbol{v} \rangle + \Delta t \, \langle \boldsymbol{B}(\tilde{\boldsymbol{u}})\bar{\boldsymbol{u}}, \boldsymbol{v} \rangle + \nu \Delta t \, \langle \nabla \bar{\boldsymbol{u}}, \nabla \boldsymbol{v} \rangle + \Delta t \, \langle p, \nabla \cdot \boldsymbol{v} \rangle - \Delta t \, \langle \boldsymbol{f}_n, \boldsymbol{v} \rangle = 0\,, \tag{7}$$

$$\langle \nabla \cdot \boldsymbol{u}_n, q \rangle = 0\,, \tag{8}$$

$$\forall (\boldsymbol{v}, q) \in W\,, \tag{9}$$

where $\langle \cdot, \cdot \rangle$ is the L^2 inner product.

2.2.4. Boundary Conditions Dirichlet boundary conditions prescribe the inflow velocity. The inflow boundaries are dynamically chosen based on the wind direction. For example, for a wind from the north-west direction, the north and west boundaries are marked as inflow. The other boundaries are given no-stress, or Neumann, conditions by default. For a three-dimensional flow case, the bottom, surface, boundary is given a no-slip Dirichlet condition.

2.2.5. Initial Conditions The model is initialised with a uniform flow-field with the initial velocity and a constant pressure. Flow structures, like wakes, naturally develop as the simulation progresses.

2.2.6. Turbulence model A generalised mixing length model is used to model the sub-grid-scale eddy viscosity. The total viscosity ν is calculated from the kinematic viscosity of air ν_0 and the viscosity due to turbulence ν_T,

$$\nu = \nu_0 + \nu_\mathrm{T} = \nu_0 + l_\mathrm{m}^2 \sqrt{\frac{1}{2}\left(\nabla \boldsymbol{u} + \nabla \boldsymbol{u}^\mathrm{T}\right)^2}\,, \tag{10}$$

where l_m is the Prandtl mixing length.

2.2.7. Turbine Model The wind turbine forcing on the flow is approximated using an actuator disk model, applied using a smoothly differentiable forcing kernel as in [10].

3. Model Evaluation

Section 3.1 outlines the wind farm configuration and flow conditions for the test cases, which are simulated using the new control model, SOWFA, and FLORIS, as described in Section 3.2.

3.1. Test Cases

We test the flow results from the model for two different cases, one steady and one with time-varying inflow. All tests use the DTU 10MW turbine with a 178.4 m diameter and 119 m hub height [14].

3.1.1. Two Turbines Under Steady Inflow The 2 km × 1 km simulation domain for the steady flow case is illustrated in Figure 2a, with an overview of simulation properties listed in Table 1. The wind flows into the domain from the west side, $\theta = 270°$, with a constant velocity $8.0\,\mathrm{m\,s^{-1}}$. The two turbines are spaced 900 m, approximately 5 D, apart and yawed to be aligned with the main wind direction.

Table 1: Simulation properties for the two test cases.

	Steady	Time-Varying
Turbine grid	2×1	3×3
Turbine spacing	900 m	900 m
Wind speed	$8\,\mathrm{m\,s^{-1}}$	$8\,\mathrm{m\,s^{-1}}$
Wind direction	270°	255° → 195°

3.1.2. Wind Farm Under Time-Varying Inflow The time-varying flow condition is tested with a 3 km × 3 km domain as illustrated in Figure 2b, with an overview of simulation properties listed in Table 1. The wind flows with a constant velocity of $8.0\,\mathrm{m\,s^{-1}}$, but rotates over time over a 60° angle as follows:

$$\theta = 255° \qquad \text{for } t < 300.0\,\mathrm{s}\,, \tag{11}$$

$$\theta = 255 - 0.2t \qquad \text{for } 300.0\,\mathrm{s} \le t \le 600.0\,\mathrm{s}\,, \tag{12}$$

$$\theta = 195° \qquad \text{for } t > 600.0\,\mathrm{s}\,. \tag{13}$$

The turbine yaw angles are fixed so that they are aligned with a wind direction of $\theta = 225°$. The inflow starts from left and rotates to the right of the turbines. These wind directions are chosen to avoid switching inflow boundaries while facilitating time-varying wind direction. The turbines are arranged in a regular 3×3 grid with a spacing of 900 m, approximately 5 D, in both directions.

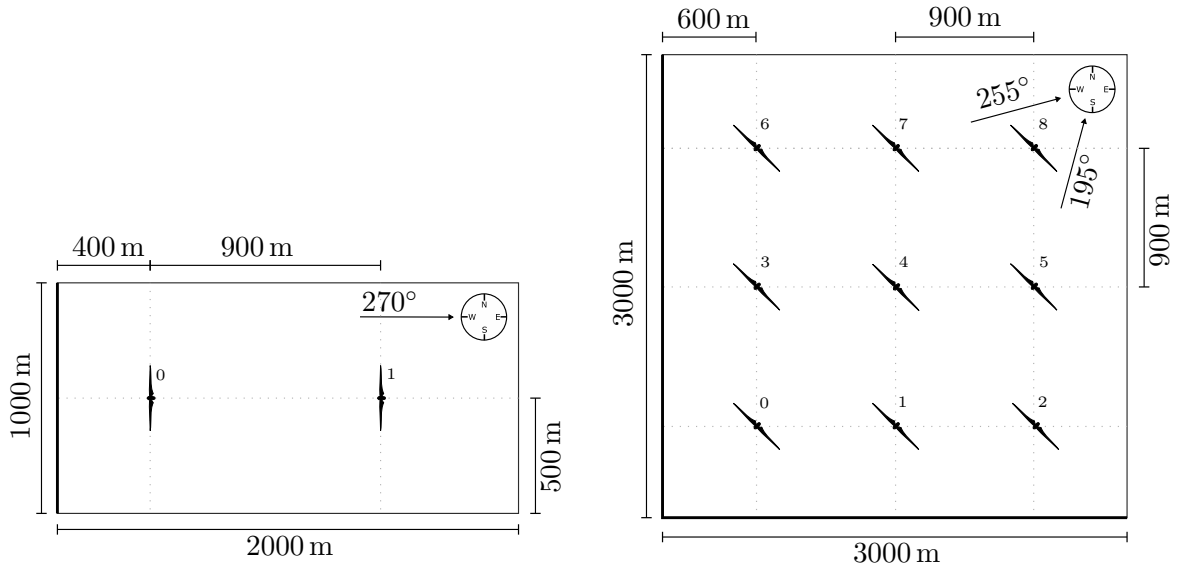

(a) Two-turbine array.

(b) Nine-turbine array.

Figure 2: Illustration of turbine array layout and domains for simulation. 2a shows the 2 km × 1 km domain with two turbines and steady inflow from the west ($\theta = 270°$). 2b shows the 3 km × 3 km domain with an array of nine turbines and time-varying inflow across south and west borders ($195° \leq \theta \leq 255°$).

3.2. Simulations

3.2.1. Control Model The control model is run on a coarse mesh with 100 m × 100 m triangular cells. The mesh is once refined around the turbine positions, yielding 50 m × 50 m cells. The time-step for integration is set to $\Delta t = 1.0$ s. The numerical parameters are listed next to the SOWFA parameters in Table 2.

3.2.2. SOWFA The high fidelity simulations for validation are run using the SOWFA simulator with turbulent precursors with a turbulence intensity of approximately 6 %. We take a horizontal slice at hub height for comparison with the two-dimensional flow results. The two-turbine case is run with a 2 km × 1 km × 0.65 km domain and the nine-turbine case with a domain size of 3 km × 3 km × 1 km. The mesh has 10 m × 10 m × 10 m cells, which are twice refined to yield 2.5 m × 2.5 m × 2.5 m cells around the turbine positions. The time-step for integration is set to $\Delta t = 0.2$ s. The turbines are modelled using an actuator line model (ALM).

Table 2: Numerical properties

	SOWFA	Control Model
Turbine model	ALM	ADM
Base cells	10 m × 10 m × 10 m	100 m × 100 m
First refinement	5 m × 5 m × 5 m	50 m × 50 m
Second refinement	2.5 m × 2.5 m × 2.5 m	–
Time-step	0.2 s	1.0 s

3.2.3. FLORIS Results from FLORIS are used to illustrate the difference between dynamic flow modelling and steady-state models currently used for wind farm control. These engineering model results are continuous in three-dimensional space. A horizontal slice at hub height is used in the comparison.

4. Results

The resulting flow field and power estimates for the steady inflow case are presented in Section 4.1, followed by the flow field results for the time-varying inflow in Section 4.2.

4.1. Two Turbines Under Steady Inflow

The flow fields for the two-turbine case are illustrated in Figure 3. The SOWFA simulation shows turbulence not present in the coarse planar flow results from the two-dimensional simulation with the new control model. For this steady inflow condition, the wake direction and magnitude are similar to the FLORIS results. The wakes calculated with the new control model are wider and show less recovery. This lack of wake recovery leads to a low flow rate through the downstream turbine.

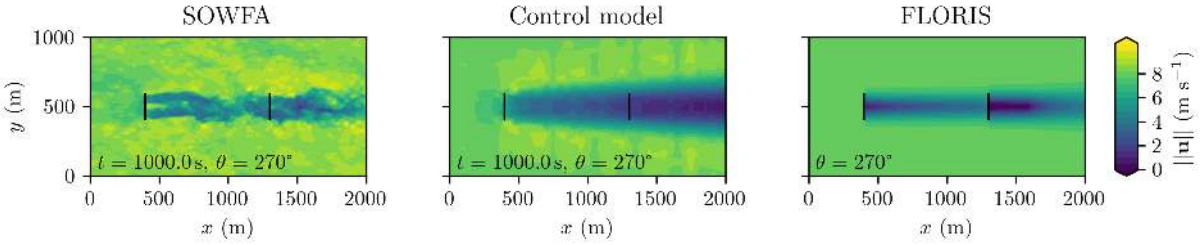

Figure 3: Two-turbine array with steady $8.0\,\mathrm{m\,s^{-1}}$ inflow from left side, as illustrated in Figure 2a. Comparing results from SOWFA with a turbulent inflow on the left, steady-state results from FLORIS on the right, and planar flow results from the new control model in the centre.

The power over time for this configuration is provided in Figure 4, with the mean power over the final 600 s listed in Table 3. The FLORIS model consistently underestimates the power compared to the high fidelity simulations. The new control model follows a trend similar to the SOWFA results for the first turbine, albeit with less disturbance because of the uniform inflow. It approximates the mean power to within 15 % in steady state. The power generated by the second turbine is lower because of the lack of wake recovery.

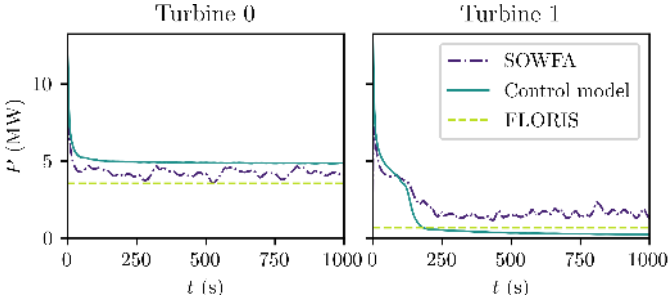

Figure 4: Power development over time.

Table 3: Mean power over last 600 s for the two-turbine case with steady inflow.

	P_0	P_1	
SOWFA	4.20	1.59	MW
Control model	4.87	0.29	MW
FLORIS	3.54	0.67	MW

4.2. Wind Farm Under Time-Varying Inflow

Figure 5 shows the flow fields as they develop over time under time-varying wind direction. The new control model exhibits a time delay as the changing wind direction propagates through the domain with the flow velocity. This behaviour differs from the high fidelity simulations, where the change in wind direction affects the whole domain simultaneously. There is still a delay before the entire wake is aligned with the new flow direction, but this alignment takes a lot less time than in the new control model. Another difference is the presence of a large speed-up effect around the turbines for the two-dimensional results in the control model, which is not present in the three-dimensional reference flow.

The FLORIS steady-state approach instantly switches wake direction as the inflow direction changes; there is no delay in the wake propagation with wind flow velocity. This delay is clearly present in the wakes modelled using the dynamic control model and SOWFA.

A comparison of the computational cost of the three simulation strategies is provided in Table 4. The SOWFA simulations run a lot slower than real-time, whereas both the control model and FLORIS yield results at a real-time order of magnitude.

Table 4: Computational efficiency $t_{\text{core}}/t_{\text{sim}}$

	SOWFA		Control model		FLORIS	
Steady	2.9×10^3	$\text{s}\,\text{s}^{-1}$	0.3	$\text{s}\,\text{s}^{-1}$	0.15	s
Time-varying	2.7×10^4	$\text{s}\,\text{s}^{-1}$	2.4	$\text{s}\,\text{s}^{-1}$	0.4	s

5. Discussion

The model performance under steady flow conditions is discussed in Section 5.1, followed by the time-varying conditions in Section 5.2. The steps for future work are outlined in Section 5.3.

5.1. Steady Flow Conditions

Under steady inflow conditions, both FLORIS and the new control model describe the wake behaviour as shown in Figure 3. Both discard the turbulent dynamics that is present in the high-fidelity SOWFA simulations, whilst still providing a good representation of the turbine wake that could be used for control optimisation. Additionally, the control model shows a power curve over time, Figure 4, that relates well to the high fidelity simulations.

Improvements to the control model are necessary because the wake width is overestimated. This is a property of the two-dimensional continuity conditions, which may be adjusted using a correction factor as in WFSim. Furthermore, wake recovery needs to be addressed for power estimates on downstream turbines.

5.2. Time-Varying Inflow Conditions

The results for time-varying flow behaviour as shown in Figure 5 show that even though the control model uses a coarse approach to flow simulation, it still captures wake dynamics that

are relevant for control signal generation.

There seems to be a fundamental difference between SOWFA and the new control model in the way that changes at the boundaries propagate throughout the flow domain. The entire domain is quickly affected by the rotating inflow in the high fidelity simulations; the turbine wakes towards the rear of the wind farm are affected at the same time as the front row of turbines. On the contrary, the new control model exhibits larger delays as the new wind conditions propagate through the domain with the flow velocity, first affecting the front row of turbines.

This difference appears to result from a different approach to the boundary conditions of the flow, where SOWFA includes pressure conditions from the precursor and the control model has only a specified inflow velocity. Comparison with field data of wind farms under time-varying conditions is necessary to find which approach best matches reality.

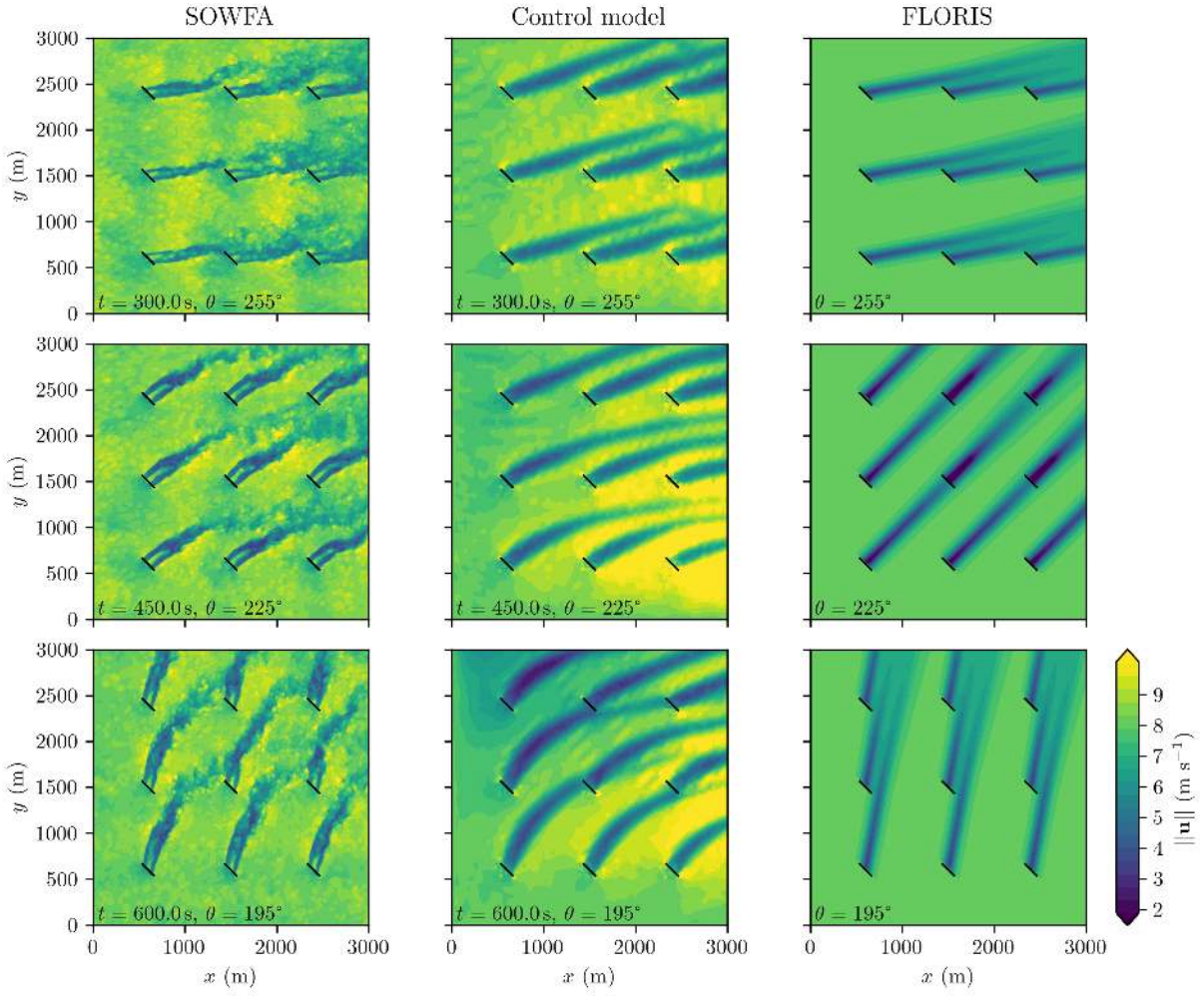

Figure 5: Three-by-three turbine array under time-varying inflow, as illustrated in Figure 2b. Comparing results from SOWFA with a turbulent inflow on the left, steady-state results from FLORIS on the right, and planar flow results from the new control model in the centre. The results from the control model show dynamic effects from time-varying wind direction, but differ from the SOWFA results in the way that changes propagate through the farm. The steady flow results from FLORIS do not show the time-variation that is present in the other flow field results.

The dynamic behaviour is the main difference with the steady-state results, which neglect temporal dynamics and are therefore unable to account for time-variations. The implementation of this dynamic control model is important to facilitate control in changing inflow conditions, however further validation is required on the accuracy of the wake dynamics.

5.3. Future Work

The model should be further developed to more accurately represent flow results under time-varying conditions, for example using field data. Additionally, the continuity corrections from WFSim may be generalized and implemented in the control model to correct wake width. A variable mixing length may be applied to adjust the wake recovery.

After these adjustments and a further step of validation on the results from the control model and high fidelity simulations, the next step is working towards a wind farm controller. We need to work on further runtime optimisation and make use of the automated adjoint calculations to optimise yaw control signals and construct a model-predictive wind farm controller around this model.

6. Conclusion

We construct a dynamic wind farm model from first principles and illustrate its place in a closed-loop wind farm controller. The model is implemented on a coarse mesh and shows dynamic flow behaviour in wake propagation. It provides a flexible basis for the development of new wind farm control strategies.

Some model adjustments are required to accurately represent three-dimensional flow in a two-dimensional model. Future work will include further validation of the dynamic flow results, the generation of optimal controls using this model, closing the feedback loop with state estimation, and testing a complete closed-loop economic model-predictive control strategy.

Acknowledgments

This work is part of the research programme "Robust closed-loop wake steering for large densely space wind farms" with project number 17512, which is (partly) financed by the Dutch Research Council (NWO).

References

[1] Gebraad P M O, Teeuwisse F W, van Wingerden J W, Fleming P A, Ruben S D, Marden J R and Pao L Y 2016 *Wind Energy* **19** 95–114

[2] van Dijk M T, van Wingerden J W, Ashuri T and Li Y 2017 *Energy* **121** 561–569 ISSN 03605442 URL `http://dx.doi.org/10.1016/j.energy.2017.01.051`

[3] Campagnolo F, Petrović V, Schreiber J, Nanos E M, Croce A and Bottasso C L 2016 *J. Phys. Conf. Ser.* **753** ISSN 17426596

[4] Fleming P, King J, Dykes K, Simley E, Roadman J, Scholbrock A, Murphy P, Lundquist J K, Moriarty P, Fleming K, van Dam J, Bay C, Mudafort R, Lopez H, Skopek J, Scott M, Ryan B, Guernsey C and Brake D 2019 *Wind Energy Sci.* **4** 273–285 ISSN 23667451

[5] Howland M F, Lele S K and Dabiri J O 2019 *Proc. Natl. Acad. Sci. U. S. A.* **116** 14495–14500 ISSN 10916490

[6] Munters W and Meyers J 2018 *Energies* **11** ISSN 19961073

[7] Boersma S, Doekemeijer B M, Vali M, Meyers J and van Wingerden J W 2018 *Wind Energy Sci.* **3** 75–95

[8] van Wingerden J W, Pao L, Aho J and Fleming P 2017 *IFAC-PapersOnLine* **50** 4484–4491 ISSN 24058963 URL `https://doi.org/10.1016/j.ifacol.2017.08.378`

[9] van Wingerden J W, Fleming P A, Göçmen T, Eguinoa I, Doekemeijer B M, Dykes K, Lawson M, Simley E, King J, Astrain D, Iribas M, Bottasso C L, Meyers J, Raach S, Kölle K and Giebel G 2020 (*Preprint* 2006.07598) URL http://arxiv.org/abs/2006.07598

[10] King R N, Dykes K, Graf P and Hamlington P E 2017 *Wind Energy Sci.* **2** 115–131

[11] Logg A, Mardal K A, Wells G N *et al.* 2012 *Automated Solution of Differential Equations by the Finite Element Method* (Springer) ISBN 978-3-642-23098-1

[12] Farrell P E, Ham D A, Funke S W and Rognes M E 2013 *SIAM J. Sci. Comput.* **35** 1–27 ISSN 10648275 (*Preprint* 1204.5577)

[13] Simo J C and Armero F 1994 *Comput. Methods Appl. Mech. Eng.* **111** 111–154 ISSN 00457825

[14] Bak C, Bitsche R, Yde A, Kim T, Hansen M H, Zahle F, Gaunaa M, Blasques J, Døssing M, Heinen J J W and Behrens T 2012 *Eur. Wind Energy Conf. Exhib. 2012* **1** 532–541